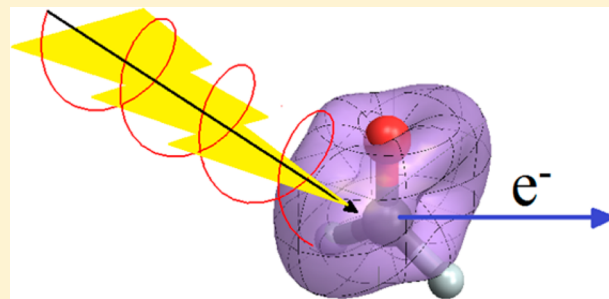


Angular Dependence of Ionization by Circularly Polarized Light Calculated with Time-Dependent Configuration Interaction with an Absorbing Potential

Paul Hoerner and H. Bernhard Schlegel*

Department of Chemistry, Wayne State University, Detroit, Michigan 48202, United States

ABSTRACT: The angular dependence of ionization by linear and circularly polarized light has been examined for N₂, NH₃, H₂O, CO₂, CH₂O, pyrazine, methyloxirane, and vinylloxirane. Time-dependent configuration interaction with single excitations and a complex absorbing potential was used to simulate ionization by a seven cycle 800 nm cosine squared pulse with intensities ranging from 0.56×10^{14} to 5.05×10^{14} W cm⁻². The shapes of the ionization yield for linearly polarized light can be understood primarily in terms of the nodal structure of the highest occupied orbitals. Depending on the orbital energies, ionization from lower-lying orbitals may also make significant contributions to the shapes. The shapes of the ionization yield for circularly polarized light can be readily explained in terms of the shapes for linearly polarized light. Averaging the results for linear polarization over orientations perpendicular to the direction of propagation yields shapes that are in very good agreement with direct calculations of the ionization yield by circularly polarized light.



INTRODUCTION

Electron dynamics plays a fundamental role in the interaction of matter with very short, intense laser pulses.^{1–3} The angular dependence of ionization in the barrier suppression regime and in the tunneling regime depends on electron dynamics on an attosecond and femtosecond time scale. The ionization rates for N₂ and CO differ significantly when the polarization of the laser field is aligned parallel versus perpendicular to the molecular axis.^{4,5} Angle-dependent ionization yields have been observed for CO₂, butadiene, and some larger polyatomics.^{6–10} High harmonic generation (HHG) spectra can also yield information about the dependence of electron dynamics on the orientation of the molecule in the laser field. HHG data and orbital tomography can be used to reconstruct the shape of the highest occupied molecular orbital (HOMO).¹¹ Circularly polarized light can lead to significantly different dynamics than linearly polarized light. For example, HHG and nonsequential double ionization are suppressed as the ellipticity of the laser pulse is changed from linear to circular. Attosecond angular streaking employing elliptically polarized light has been used to measure ionization delay with an accuracy of tens of attoseconds.¹² Currently, there is great interest in applying the angular streaking method to molecular systems to observe attosecond electronic dynamics.¹³ This will require theoretical methods that can properly and efficiently model the angular-dependent ionization of molecules by circularly polarized light. In the present work, we compare the angular dependence of ionization by short, intense pulses of linear and circularly polarized light.

The nodal structure of the molecular orbitals provides a qualitative description of the angular dependence of ionization

for simple molecules. A better description of ionization in the tunneling regime can be obtained with molecular Ammosov–Delone–Krainov (ADK) theory.^{14,15} More quantitative descriptions of HHG spectra and the angular dependence of ionization are provided by solving the time-dependent Schrödinger equation (TDSE) using approximations such as single active electron, quantitative rescattering theory, time-dependent resolution in ionic states, time-dependent analytical R-matrix, and time-dependent generalized active space configuration interaction.^{16–20} In previous studies, we have used a time-dependent configuration interaction (TDCI) approach with atom-centered basis functions and a complex absorbing potential (CAP) to examine the angular dependence of strong-field ionization by linearly polarized light for N₂, O₂, CO₂, and CH₂O, a set of polyenes, a series of second and third period hydrides, and various triply bonded systems.^{21–24} In this study, we examine the angular dependence of ionization of N₂, NH₃, H₂O, CO₂, CH₂O, pyrazine, methyloxirane, and vinylloxirane by linear and circularly polarized light. We find that the shapes of the frontier orbitals govern the shapes of the ionization yields for linearly polarized light. In turn, the dependence of the ionization on the direction of propagation for circularly polarized light is in good agreement with the results from linearly polarized light averaged over directions perpendicular to the direction of propagation.

Received: November 12, 2016

Revised: January 16, 2017

Published: January 18, 2017



ACS Publications

© XXXX American Chemical Society

A

DOI: 10.1021/acs.jPCA.6b11415
J. Phys. Chem. A XXXX, XXX, XXX–XXX

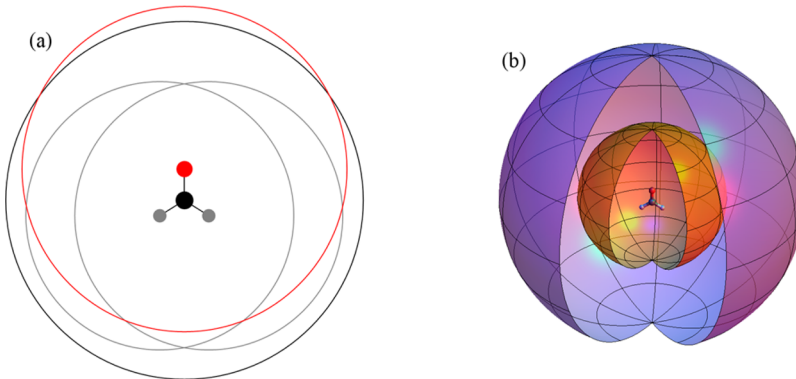


Figure 1. CAP for formaldehyde, (a) made up of the union of spheres of radii R_H , R_O , and R_C centered on each atom; (b) three-dimensional shape of the CAP for formaldehyde, the orange surface depicting the beginning of the CAP and the purple surface at the radius where the CAP has risen to approximately 1.5 au.

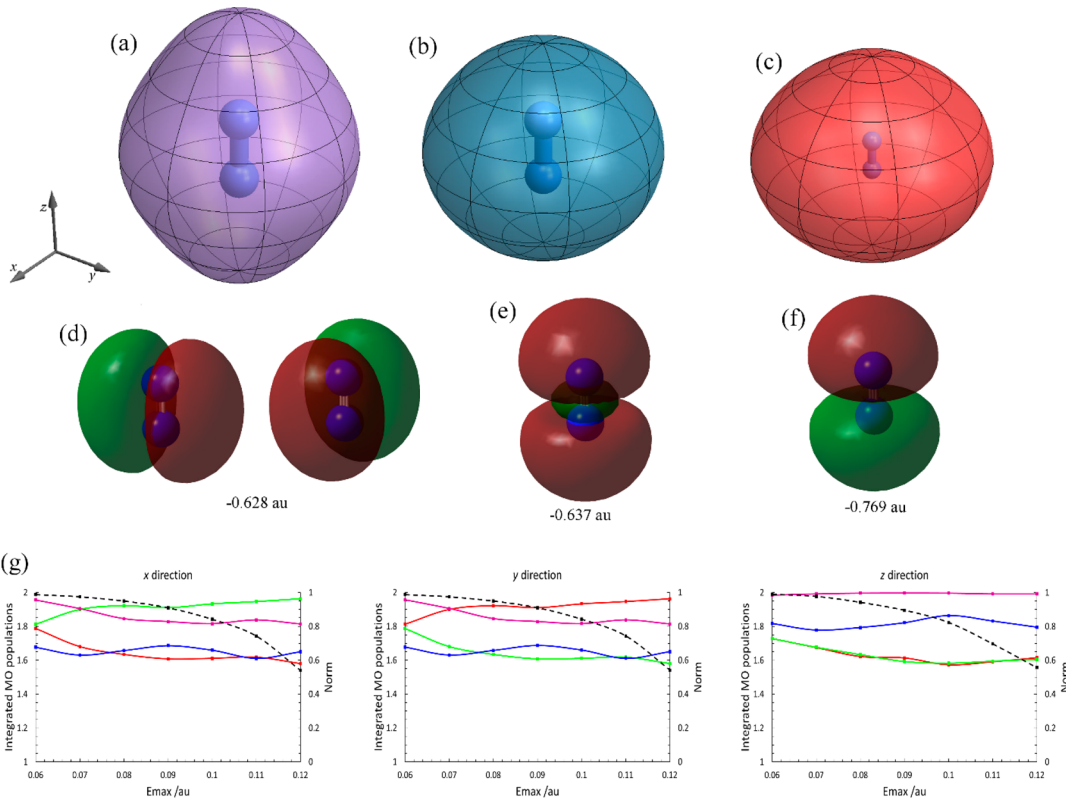


Figure 2. Angular-dependent ionization yield of N₂ for (a) linearly polarized light, (b) circular polarized light estimated from linearly polarized light, and (c) circularly polarized light at an intensity of $1.95 \times 10^{14} \text{ W cm}^{-2}$; (d) doubly degenerate HOMO, (e) HOMO-1, and (f) HOMO-2; (g) orbital populations as a function of field strength for circularly polarized light propagating along the x , y , and z axes: HOMO (red and green), HOMO-1 (blue), and HOMO-2 (purple); the final norm of the neutral wave function as a function of field strength (dashed black, right axis).

METHODS

The electron dynamics were simulated by solving the TDSE

$$i\frac{\partial}{\partial t}\Psi_{el}(t) = [\hat{H}_{el} - \hat{\vec{\mu}} \cdot \vec{E}(t) - i\hat{V}^{\text{absorb}}]\Psi_{el}(t) \quad (1)$$

where \hat{H}_{el} is the field-free electronic Hamiltonian. The interaction between electron and light is modeled using the semi-classical dipole approximation, where $\hat{\vec{\mu}}$ is the dipole operator and \vec{E} is the electric field component of the laser pulse. A CAP, $-i\hat{V}^{\text{absorb}}$, is used to model ionization as described in our

previous papers.^{21–25} The absorbing potential is constructed from a set of overlapping spherical potentials centered around each atom, as shown in Figure 1a. The total absorbing potential for the molecule is equal to the minimum of the values of the atomic absorbing potentials. Each spherical potential begins at 3.5 times the van der Waals radius of each element ($R_H = 5.051 \text{ \AA}$, $R_C = 6.739 \text{ \AA}$, $R_N = 6.405 \text{ \AA}$, $R_O = 6.125 \text{ \AA}$); after a quadratic start, it rises linearly to a quadratic turnover to constant value of 10 hartree at approximately $R + 50 \text{ \AA}$. For many of the small molecules in this study, the CAP is nearly spherical (Figure 1b).

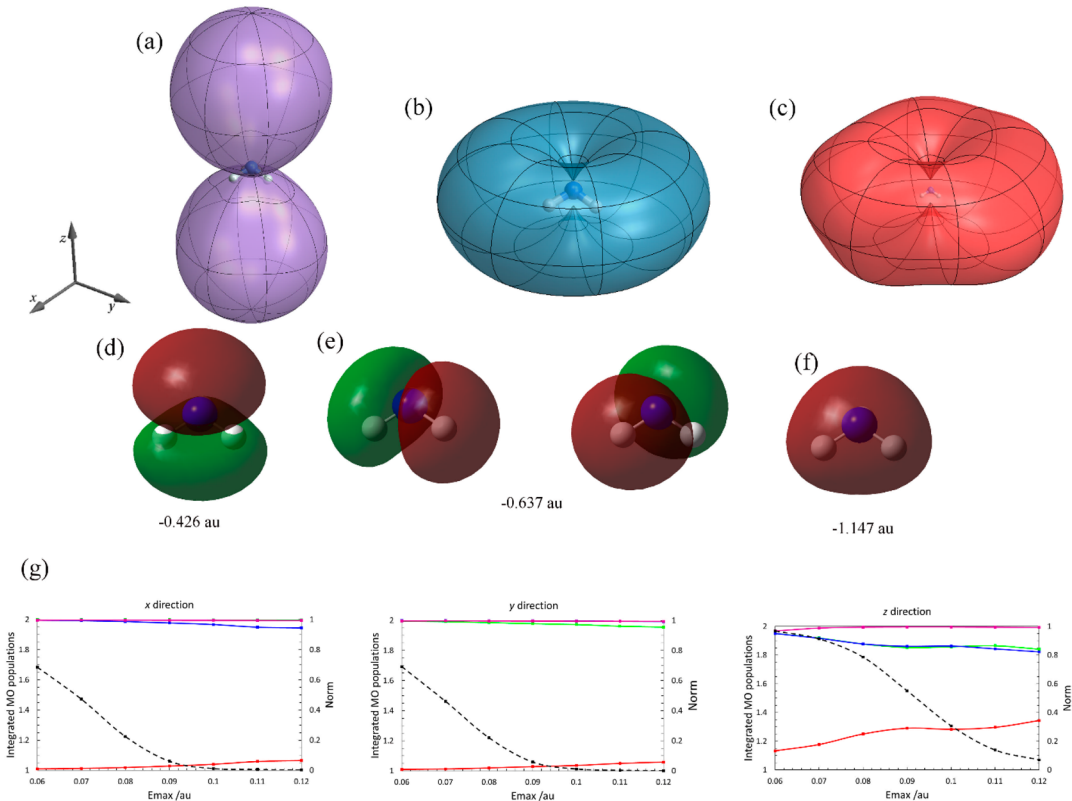


Figure 3. Angular-dependent ionization yield of NH₃ for (a) linearly polarized light, (b) circular polarized light estimated from linearly polarized light, and (c) circularly polarized light at an intensity of $1.44 \times 10^{14} \text{ W cm}^{-2}$; (d) HOMO, (e) the doubly degenerate HOMO-1, and (f) HOMO-2; (g) orbital populations as a function of field strength for circularly polarized light propagating along the *x*, *y*, and *z* axes: HOMO (red), HOMO-1 (green and blue), and HOMO-2 (purple); the final norm of the neutral wave function as a function of field strength (dashed black, right axis).

The electric field for a circularly polarized cosine squared pulse is given by

$$\begin{aligned}\vec{E}(t) &= \vec{E}_1(t) + \vec{E}_2(t) \quad \text{for } -\sigma \leq t \leq \sigma, \quad \vec{E}(t) = 0 \text{ otherwise} \\ \vec{E}_1(t) &= E_{\max} \vec{e}_1 \cos^2(\pi t / 2\sigma) \sin(\omega t - \phi) \\ \vec{E}_2(t) &= E_{\max} \vec{e}_2 \cos^2(\pi t / 2\sigma) \cos(\omega t - \phi)\end{aligned}\quad (2)$$

where \vec{e}_1 and \vec{e}_2 are mutually orthogonal unit vectors that are perpendicular to the direction of propagation of the pulse.

The time-dependent wave function is expanded in the basis of the Hartree–Fock ground state and all singly excited states of the field-free, time-independent Hamiltonian.

$$\Psi(t) = \sum_{i=0} C_i(t) |\Psi_i\rangle \quad (3)$$

A Trotter factorization of the exponential of the Hamiltonian is used to propagate the time-dependent wave function

$$\begin{aligned}\Psi(t + \Delta t) &= \exp(-i\hat{H}\Delta t)\Psi(t) \\ C(t + \Delta t) &= \exp(-iH_{\text{el}}\Delta t/2) \exp(-V^{\text{absorb}}\Delta t/2) \\ &\times \mathbf{W}_2^T \exp(i\vec{E}_2(t + \Delta t/2) \cdot \mathbf{d}_2 \Delta t/2) \mathbf{W}_2 \\ &\times \mathbf{W}_1^T \exp(i\vec{E}_1(t + \Delta t/2) \cdot \mathbf{d}_1 \Delta t) \mathbf{W}_1 \\ &\times \mathbf{W}_2^T \exp(i\vec{E}_2(t + \Delta t/2) \cdot \mathbf{d}_2 \Delta t/2) \mathbf{W}_2 \\ &\times \exp(-V^{\text{absorb}}\Delta t/2) \exp(-iH_{\text{el}}\Delta t/2) \mathbf{C}(t)\end{aligned}\quad (4)$$

where $\mathbf{W}_1 \mathbf{D}_1 \mathbf{W}_1^T = \mathbf{d}_1$ and $\mathbf{W}_2 \mathbf{D}_2 \mathbf{W}_2^T = \mathbf{d}_2$ are the eigenvalues and eigenvectors of the transition dipole matrices \mathbf{D}_1 and \mathbf{D}_2 in

the \vec{e}_1 and \vec{e}_2 directions. \mathbf{W}_1 , \mathbf{W}_2 , \mathbf{d}_1 , \mathbf{d}_2 , $\exp(-iH_{\text{el}}\Delta t/2)$, and $\exp(-V^{\text{absorb}}\Delta t/2)$ need to be calculated only once because they are time-independent. The propagation for circular polarized light involves the exponential of two diagonal matrices, \mathbf{d}_1 and \mathbf{d}_2 , and four matrix–vector multiplies. For linearly polarized light, the \mathbf{W}_2 and \mathbf{d}_2 factors are omitted and the propagation involves only two matrix–vector multiplies. A time step of $\Delta t = 0.05 \text{ au}$ (1.2 as) was used. Reducing the time step by a factor of 2 changed the norm at the end of the pulse by less than 0.01% for formaldehyde with a field strength of 0.06 au. Interchanging the dipole-dependent terms in the Trotter factorization changed the norm at the end of the pulse by less than 0.5% for $\Delta t = 0.05 \text{ au}$ and 0.5% for $\Delta t = 0.025 \text{ au}$.

The electronic structure calculations necessary for the TDCIS simulations were carried out using a modified version of the Gaussian software package.²⁶ The Dunning aug-cc-pVTZ basis set^{27,28} was augmented with a basis of extra diffused functions for adequate interaction with the CAP. This additional basis consisted of nine sets of diffuse Gaussian functions on each atom (including hydrogen): three s functions (with exponents 0.0256, 0.0128, and 0.0064), two sets of p functions (0.0256 and 0.0128), three sets of d functions (0.0512, 0.0256, and 0.0128), and one set of f functions (0.0256). Additional details of the development and validation of this absorbing basis can be found in ref 25.

The simulations used a seven cycle pulse with a frequency of $0.057E_h/\hbar$ (800 nm) and $\phi = \pi$. The system was propagated for a total of $800\hbar/E_h$ (19.4 fs) with intensities ranging from 0.56×10^{14} to $5.05 \times 10^{14} \text{ W cm}^{-2}$ (electric field strengths from 0.04 to 0.12 au). The ionization potentials for the molecules

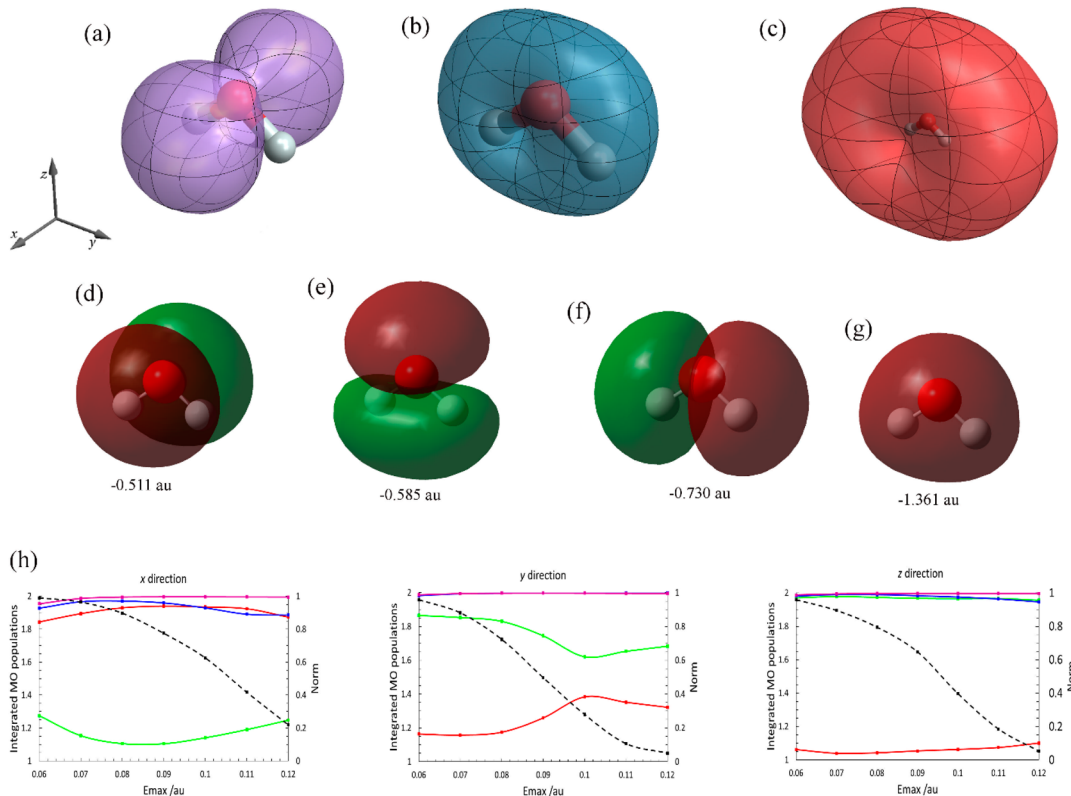


Figure 4. Angular-dependent ionization yield of H₂O for (a) linearly polarized light, (b) circular polarized light estimated from linearly polarized light, and (c) circularly polarized light at an intensity of $1.95 \times 10^{14} \text{ W cm}^{-2}$; (d) HOMO, (e) HOMO-1, (f) HOMO-2, and (g) HOMO-3; (h) orbital populations as a function of field strength for circularly polarized light propagating along the *x*, *y*, and *z* axes: HOMO (red), HOMO-1 (green), HOMO-2 (blue), and HOMO-3 (purple); the final norm of the neutral wave function as a function of field strength (dashed black, right axis).

considered in this study range from 0.35 to 0.57 au, and ionization at these intensities occurs primarily by barrier suppression as opposed to tunneling. When the field returns to zero after the pulse, the loss of norm is taken as the ionization yield for that pulse. Varying the direction of propagation and polarization of the pulse for a given E_{max} results in a three-dimensional surface that is interpreted as the angle-dependent ionization rate. The spherical angles θ and ϕ were changed in steps of 30° for a total of 62 points for each E_{max} . To obtain smooth surfaces for plotting, ionization yields were fitted to polynomials in $\cos(\theta)^n \cos(m\phi)$ and $\cos(\theta)^n \sin(m\phi)$, $n = 0-7$, $m = 0-6$.

RESULTS AND DISCUSSION

Figures 2–9 show the angular-dependent ionization yields for N₂, NH₃, H₂O, CO₂, CH₂O, pyrazine (C₄N₂H₄), methyloxirane (C₃H₆O), and vinyloxirane (C₄H₆O), respectively. The ionization yield is taken as the decrease in the norm of the wave function after the pulse and is plotted as the distance from the origin as a function of the angle of polarization of the light for linearly polarized light and as a function of the direction of propagation of light for circularly polarized light. An estimate of the angular dependence of ionization by circularly polarized light was also obtained by averaging the ionization yield for linearly polarized light for 0–360° around the direction of propagation for circularly polarized light.

The angular-dependent ionization yield of N₂ with linearly polarized light resembles a prolate ellipsoid (Figure 2a) and can be understood in terms of the frontier molecular orbitals shown (Figure 2d–f). The doubly degenerate π-bonding HOMO and

the symmetric σ lone pair HOMO-1 are very close in energy and contribute nearly equally to the ionization yield; the anti-symmetric σ lone pair HOMO-2 is lower in energy and contributes much less. An approximation to the ionization yield with circularly polarized light can be obtained by averaging the linearly polarized results around the direction of propagation. The result at this field strength is nearly spherical (Figure 2b), which is in very good agreement with the direct calculation of the ionization yield with circularly polarized light shown in Figure 2c. The contributions of the orbitals to the ionization yield for circularly polarized light propagating in the *x*, *y*, and *z* directions are shown in Figure 2g. Using the Cartesian representation for the π orbitals, one of the HOMOs and the HOMO-1 are the largest contributors for the *x* and *y* directions. The doubly degenerate HOMO is the main contributor for circularly polarized light directed along the molecular axis (*z* direction).

The results for the angular-dependent ionization of NH₃ are shown in Figure 3. The HOMO is an sp³ lone pair and is the dominant contributor to ionization; the doubly degenerate HOMO-1 and HOMO-2 are formed from the N–H bonding orbitals (Figure 3e,f). For linearly polarized light, ionization is dominated by the HOMO and has a minimum in the *xy* plane where the HOMO has a node (Figure 3a). When the linearly polarized results are averaged around the direction of propagation to obtain an approximation for ionization by circularly polarized light, the minimum in the *xy* plane produces a minimum along the *z* direction (Figure 3b). The same feature is seen in the direct calculation of ionization by circularly polarized light (Figure 3c), along with a slight hexagonal deformation

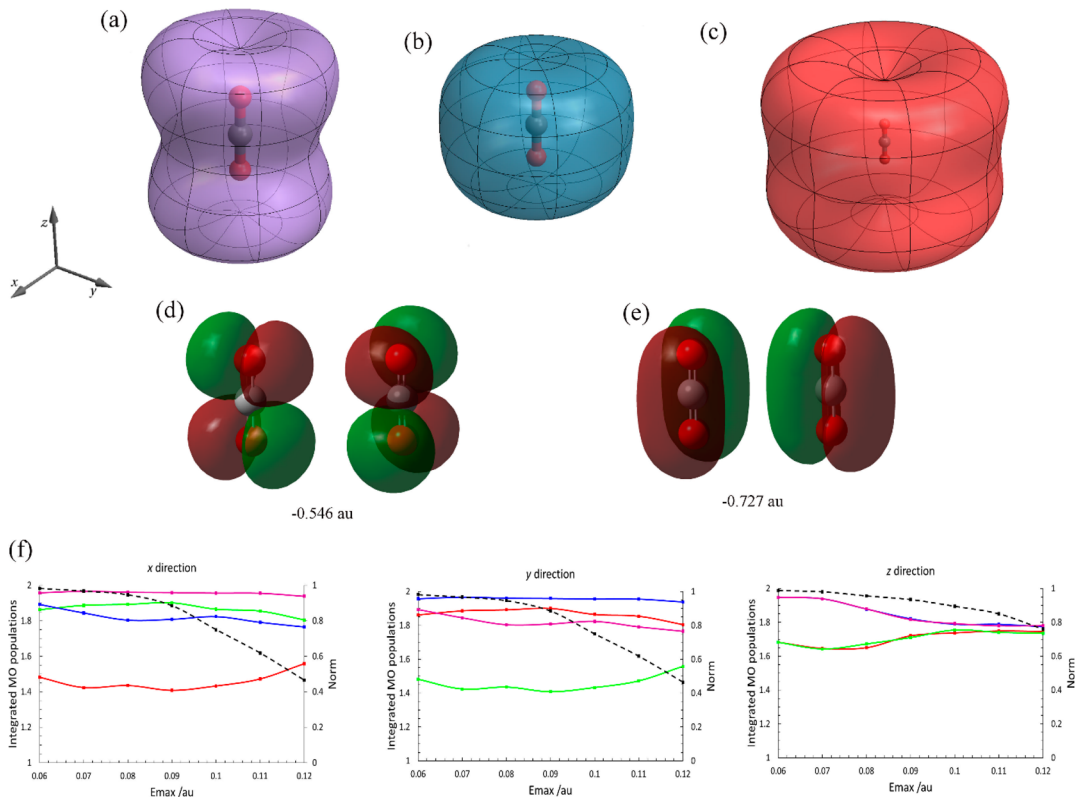


Figure 5. Angular-dependent ionization yield of CO_2 for (a) linearly polarized light, (b) circular polarized light estimated from linearly polarized light, and (c) circularly polarized light at an intensity of $1.95 \times 10^{14} \text{ W cm}^{-2}$; (d) the doubly degenerate HOMO and (e) doubly degenerate HOMO-1; (f) orbital populations as a function of field strength for circularly polarized light propagating along the x , y , and z axes: HOMO (red and green) and HOMO-1 (blue and purple); the final norm of the neutral wave function as a function of field strength (dashed black, right axis).

arising from HOMO-1 and HOMO-2. Figure 3g shows that the HOMO dominates the ionization yield from circularly polarized light propagating in the x and y directions. For circularly polarized light propagating in the z direction (i.e., when the electric field is rotating in the xy plane), the contribution of the HOMO is somewhat diminished because of the node in the xy plane. HOMO-1 and HOMO-2 make a significant contribution in the z direction but not in the x and y directions.

The results found for H_2O (Figure 4) are similar to those for NH_3 . The angular dependence of ionization is dominated by the π lone pair HOMO. As shown in Figure 4a for linearly polarized light, this yields a minimum in the plane of the molecule. When an approximation for circularly polarized light is obtained by averaging the linear polarization results around the direction of propagation, this produces a minimum for directions perpendicular to the molecular plane (Figure 4b). This shape is in good agreement with the direct calculation of the ionization yield with circularly polarized light shown in Figure 4c. For circularly polarized light propagating in the z direction, ionization occurs mostly from the HOMO (Figure 4h). Because the HOMO has a node perpendicular to the x axis, HOMO-1 is the main contributor to ionization in the x direction.

Figure 5 contains the results for angle-dependent ionization of CO_2 . The high symmetry of the molecule and the MOs leads to a cylindrically symmetrical ionization surface. The HOMO is doubly degenerate and has nodes parallel and perpendicular to the molecular axis (Figure 5d). As a result, the ionization by

linearly polarized light has a minimum along the molecular axis and a narrower waist in the xy plane (Figure 5a). When the results for linear polarization are averaged around the direction of propagation as an approximation to the angular dependence for circularly polarized light, the minimum in the xy plane leads to a small dimple along the z axis (Figure 5b). The direct calculation by circularly polarized light (Figure 5c) shows a larger dimple along the z axis and a slight narrowing at the waist in the xy plane. For propagation of circularly polarized light in the x and y directions, the doubly degenerate HOMO makes the biggest contribution. For higher field strengths in the z direction, HOMO and HOMO-1 make nearly equal contributions. Even though CO_2 and N_2 are both linear molecules, the nodal structure of the highest occupied orbitals results in distinctly different shapes for the angular dependence of ionization.

The strong field ionization results for CH_2O are presented in Figure 6. The HOMO is the dominant contributor to ionization and is the out-of-phase combination of the in-plane oxygen lone pair and the C–H bonds (Figure 6d). HOMO-1 is the C=O π bond (Figure 6e), and HOMO-2 is the oxygen σ lone pair interacting with the C–H bonds (Figure 6f). As is evident in Figure 6a, the nodal structure of the HOMO accounts for the shape of the ionization yield with linearly polarized light. Averaging the results for linearly polarized light yields a shape (Figure 6b) that is in good agreement with the direct calculation of ionization by circularly polarized light (Figure 6c). The dimple in the z direction is due to the node in the HOMO in the xy plane, and the dimple in the y direction is due to the node in the xz plane. Because the lobes of the

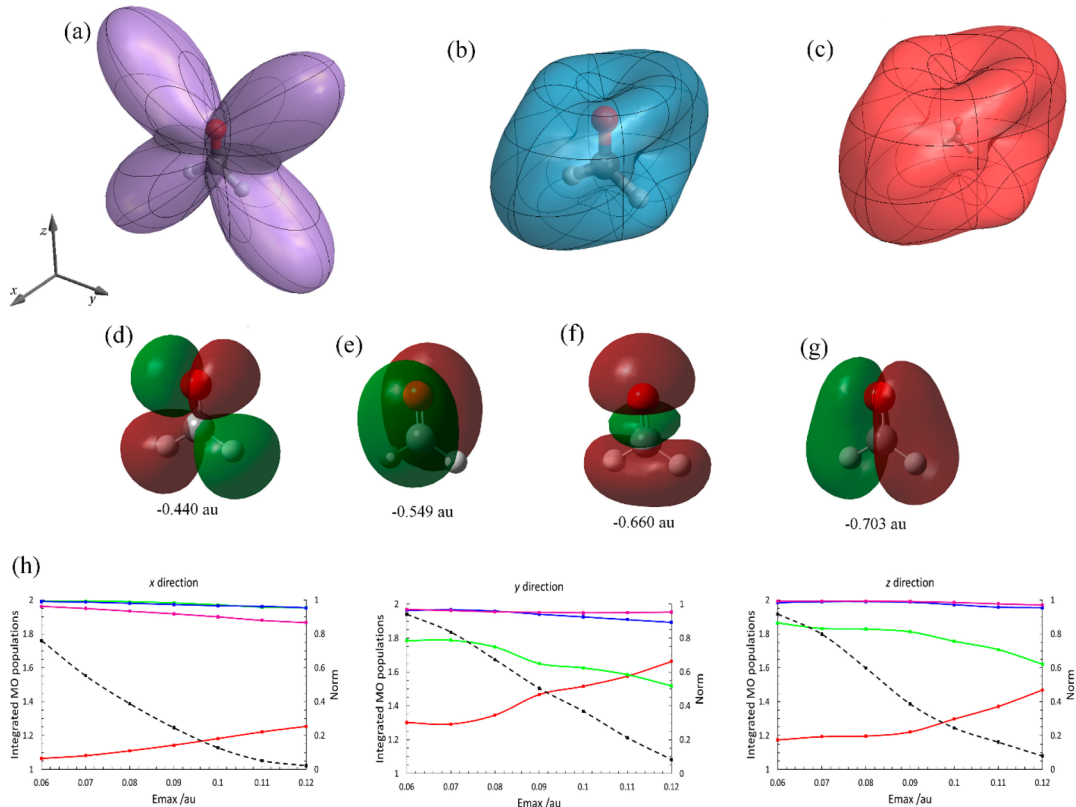


Figure 6. Angular-dependent ionization yield of CH_2O for (a) linearly polarized light, (b) circular polarized light estimated from linearly polarized light, and (c) circularly polarized light at an intensity of $1.44 \times 10^{14} \text{ W cm}^{-2}$; (d) HOMO, (e) HOMO-1, (f) HOMO-2, and (g) HOMO-3; (h) orbital populations as a function of field strength for circularly polarized light propagating along the x , y , and z axes: HOMO (red), HOMO-1 (green), HOMO-2 (blue), and HOMO-3 (purple); the final norm of the neutral wave function as a function of field strength (dashed black, right axis).

HOMO are in the yz plane, ionization by circularly polarized light is a maximum in the x direction (i.e., when the electric vector rotates in the yz plane). For circularly polarized light propagating in the y and z directions (Figure 6e), HOMO-1 makes a significant contribute to ionization because it does not have nodes in the xz and xy planes, respectively.

We have chosen pyrazine to illustrate that understanding gleaned from the small molecules also carries over to somewhat larger systems (Figure 7). The HOMO is a π orbital with a node in the plane of the molecule and another node through the two nitrogens and perpendicular to the molecular plane (Figure 7d). HOMO-1 and HOMO-3 are the in-phase and out-of-phase nitrogen lone pairs (Figure 7e,g), and HOMO-2 contains the nitrogen p_{π} orbitals (Figure 7f). Because HOMO-1, HOMO-2, and HOMO-3 are significantly lower in energy than HOMO, the shape of the ionization yield for linearly polarized light is dominated by the nodal structure of the HOMO (Figure 7a). The overall shape is similar to that of CH_2O but is oriented perpendicular to the molecular plane. Averaging the linearly polarization results around the propagation direction yields a shape (Figure 7b) that is in very good agreement with the direct calculation of ionization yield for circularly polarized light (Figure 7c). The dimples in the x and y directions for circularly polarized light are due to the minima in the yz and xz planes, respectively, for linearly polarized light. The HOMO is the main contributor in the z direction (Figure 7h), but HOMO-1 and HOMO-3 are significant contributors in the z direction.

Figure 8 shows the angle-dependent ionization for chiral molecule methyloxirane. Just as the structures for *R*- and *S*-methyloxirane are mirror images, so too are the angle dependence of the ionization yield (Figure 8a,b). Right and left circularly polarized light give essentially the same results [Figure 8 panel (a) vs (c) and panel (b) vs (d)]. The difference in the absorption of right and left circularly polarized light at 800 nm is very small for methyloxirane because this wavelength is far from lowest excitation. The ionization yields for vinyl-oxirane are shown in Figure 9. The results for *R*- and *S*-vinyl-oxirane are also mirror images. Whereas the oxygen is the main contributor to ionization in methyloxirane, the double bond is the main component of the highest occupied orbital and the dominant contributor to the ionization yield.

■ SUMMARY

The present study has examined the angular dependence of ionization by linear and circularly polarized light for a series of small molecules. The calculations used time-dependent configuration interaction with single excitations and a CAP. The simulations were carried out with a seven cycle 800 nm cosine squared pulse and intensities ranging from 0.56×10^{14} to $5.05 \times 10^{14} \text{ W cm}^{-2}$. The angular dependence of ionization was examined for N_2 , NH_3 , H_2O , CO_2 , CH_2O , pyrazine, methyloxirane, and vinyl-oxirane. These molecules provide an assortment of molecular structures, bonding motifs, and nodal patterns of the frontier orbitals. For linearly polarized light, the shape of the ionization yield as a function of the polarization direction of the laser pulse can be readily understood in

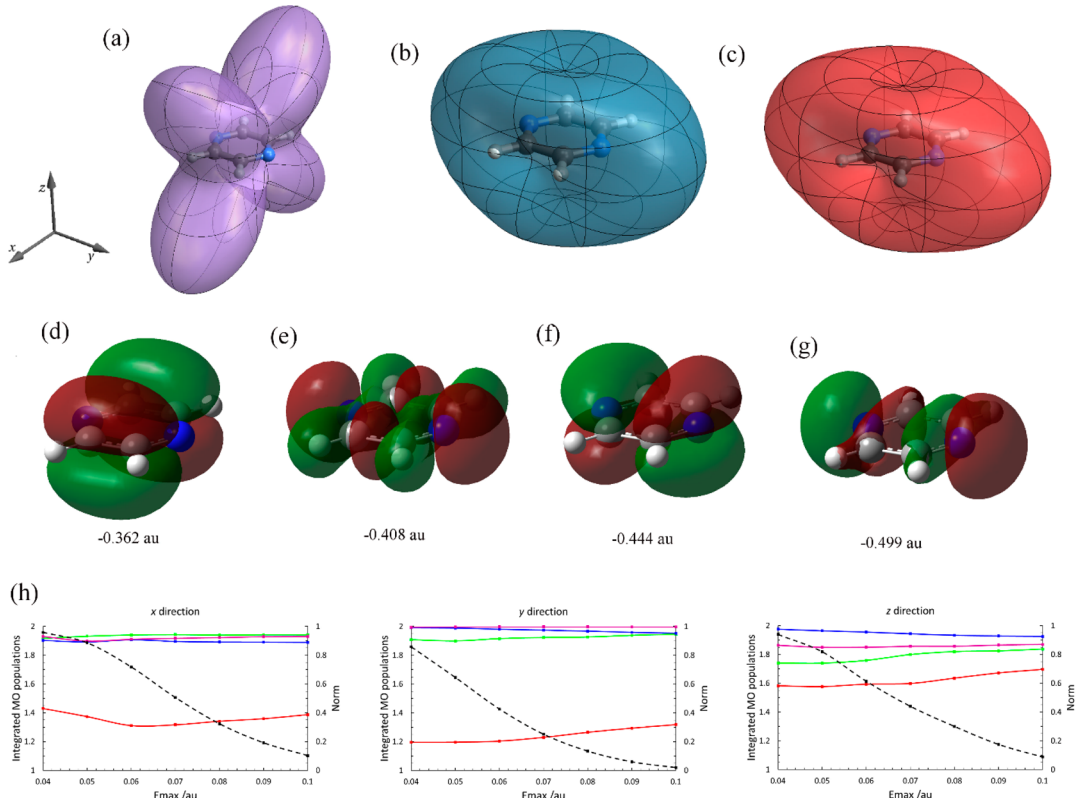


Figure 7. Angular-dependent ionization yield of pyrazine for (a) linearly polarized light, (b) circular polarized light estimated from linearly polarized light, and (c) circularly polarized light at an intensity of $0.56 \times 10^{14} \text{ W cm}^{-2}$; (d) HOMO, (e) HOMO-1, (f) HOMO-2, and (g) HOMO-3; (h) orbital populations as a function of field strength for circularly polarized light propagating along the *x*, *y*, and *z* axes: HOMO (red), HOMO-1 (green), HOMO-2 (blue), and HOMO-3 (purple); the final norm of the neutral wave function as a function of field strength (dashed black, right axis).

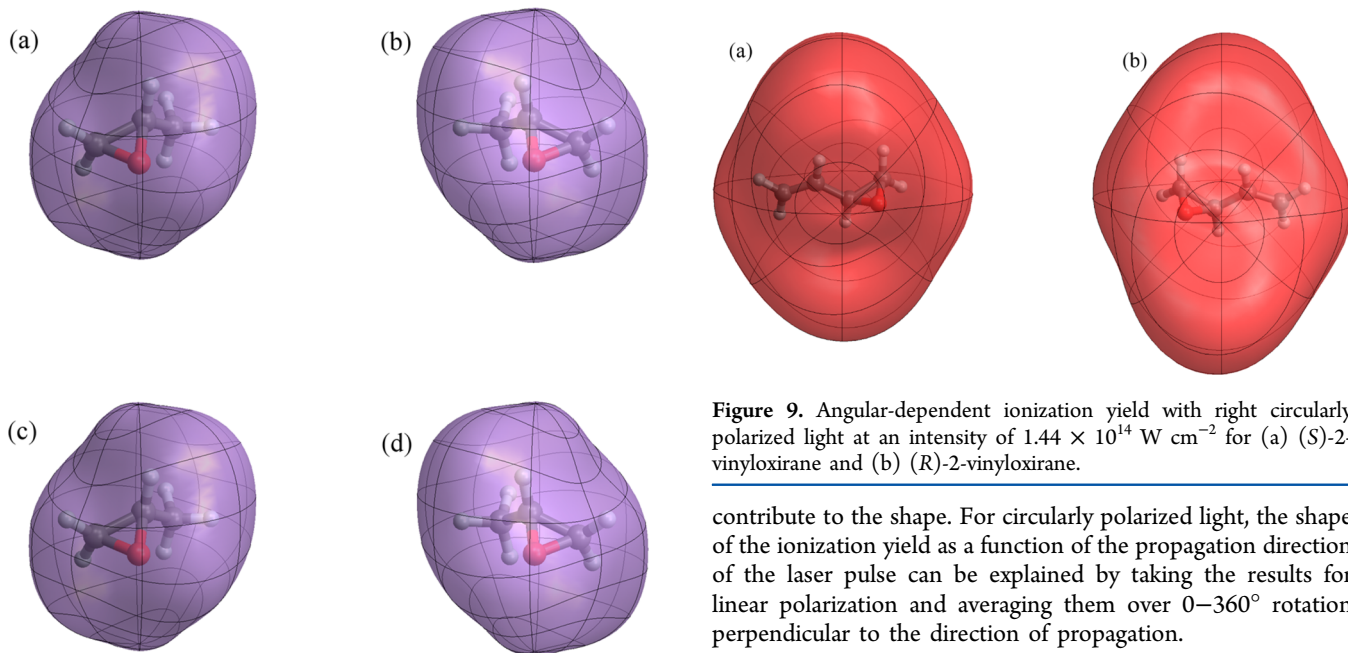


Figure 8. Angular-dependent ionization yield at an intensity of $1.44 \times 10^{14} \text{ W cm}^{-2}$ for (a) (S)-methylloxirane with right circularly polarized light, (b) (R)-methylloxirane with right circularly polarized light, (c) (S)-methylloxirane with left circularly polarized light, and (d) (R)-methylloxirane with left circularly polarized light.

terms of the nodal structure of the highest occupied orbitals. Depending on their orbital energy, lower-lying orbitals can also

Figure 9. Angular-dependent ionization yield with right circularly polarized light at an intensity of $1.44 \times 10^{14} \text{ W cm}^{-2}$ for (a) (S)-2-vinylloxirane and (b) (R)-2-vinylloxirane.

contribute to the shape. For circularly polarized light, the shape of the ionization yield as a function of the propagation direction of the laser pulse can be explained by taking the results for linear polarization and averaging them over $0\text{--}360^\circ$ rotation perpendicular to the direction of propagation.

AUTHOR INFORMATION

Corresponding Author

*E-mail: hbs@chem.wayne.edu. Tel 313-577-2562.

ORCID

H. Bernhard Schlegel: [0000-0001-7114-2821](https://orcid.org/0000-0001-7114-2821)

Notes

The authors declare no competing financial interest.

ACKNOWLEDGMENTS

This work was supported by a grant from the National Science Foundation (CHE1464450). We thank the Wayne State University computing grid for the computer time.

REFERENCES

- (1) Kling, M. F.; Vrakking, M. J. J. Attosecond electron dynamics. *Annu. Rev. Phys. Chem.* **2008**, *59*, 463–492.
- (2) Krausz, F.; Ivanov, M. Attosecond physics. *Rev. Mod. Phys.* **2009**, *81*, 163–234.
- (3) Gallmann, L.; Cirelli, C.; Keller, U. Attosecond science: Recent highlights and future trends. *Annu. Rev. Phys. Chem.* **2012**, *63*, 447–469.
- (4) Litvinyuk, I. V.; Lee, K. F.; Dooley, P. W.; Rayner, D. M.; Villeneuve, D. M.; Corkum, P. B. Alignment-dependent strong field ionization of molecules. *Phys. Rev. Lett.* **2003**, *90*, 233003.
- (5) Pinkham, D.; Jones, R. R. Intense laser ionization of transiently aligned CO. *Phys. Rev. A: At., Mol., Opt. Phys.* **2005**, *72*, 023418.
- (6) Pavicic, D.; Lee, K. F.; Rayner, D. M.; Corkum, P. B.; Villeneuve, D. M. Direct measurement of the angular dependence of ionization for N₂, O₂, and CO₂ in intense laser fields. *Phys. Rev. Lett.* **2007**, *98*, 243001.
- (7) Thomann, I.; Lock, R.; Sharma, V.; Gagnon, E.; Pratt, S. T.; Kapteyn, H. C.; Murnane, M. M.; Li, W. Direct measurement of the angular dependence of the single-photon ionization of aligned N₂ and CO₂. *J. Phys. Chem. A* **2008**, *112*, 9382–9386.
- (8) Boguslavskiy, A. E.; Mikosch, J.; Gijsbertsen, A.; Spanner, M.; Patchkovskii, S.; Gador, N.; Vrakking, M. J. J.; Stolow, A. The multielectron ionization dynamics underlying attosecond strong-field spectroscopies. *Science* **2012**, *335*, 1336–1340.
- (9) Mikosch, J.; Boguslavskiy, A. E.; Wilkinson, I.; Spanner, M.; Patchkovskii, S.; Stolow, A. Channel- and angle-resolved above threshold ionization in the molecular frame. *Phys. Rev. Lett.* **2013**, *110*, 023004.
- (10) Njoya, O.; Matsika, S.; Weinacht, T. Angle-resolved strong-field ionization of polyatomic molecules: More than the orbitals matters. *ChemPhysChem* **2013**, *14*, 1451–1455.
- (11) Itatani, J.; Levesque, J.; Zeidler, D.; Niikura, H.; Pepin, H.; Kieffer, J. C.; Corkum, P. B.; Villeneuve, D. M. Tomographic imaging of molecular orbitals. *Nature* **2004**, *432*, 867–871.
- (12) Eckle, P.; Pfeiffer, A. N.; Cirelli, C.; Staudte, A.; Dorner, R.; Muller, H. G.; Buttiker, M.; Keller, U. Attosecond ionization and tunneling delay time measurements in helium. *Science* **2008**, *322*, 1525–1529.
- (13) Eckle, P.; Smolarski, M.; Schlup, P.; Biegert, J.; Staudte, A.; Schöffler, M.; Müller, H. G.; Dörner, R.; Keller, U. Attosecond angular streaking. *Nat. Phys.* **2008**, *4*, 565–570.
- (14) Ammosov, M. V.; Delone, N. B.; Krainov, V. P. Tunnel ionization of complex atoms and of atomic ions in an alternating electromagnetic field. *Soviet Physics - JETP* **1986**, *64*, 1191–1194.
- (15) Tong, X. M.; Zhao, Z. X.; Lin, C. D. Theory of molecular tunneling ionization. *Phys. Rev. A: At., Mol., Opt. Phys.* **2002**, *66*, 033402.
- (16) Petretti, S.; Vanne, Y. V.; Saenz, A.; Castro, A.; Decleva, P. Alignment-dependent ionization of N₂, O₂, and CO₂ in intense laser fields. *Phys. Rev. Lett.* **2010**, *104*, 223001.
- (17) Le, A. T.; Lucchese, R. R.; Tonzani, S.; Morishita, T.; Lin, C. D. Quantitative rescattering theory for high-order harmonic generation from molecules. *Phys. Rev. A: At., Mol., Opt. Phys.* **2009**, *80*, 013401.
- (18) Spanner, M.; Patchkovskii, S. One-electron ionization of multielectron systems in strong nonresonant laser fields. *Phys. Rev. A: At., Mol., Opt. Phys.* **2009**, *80*, 063411.
- (19) Torlina, L.; Ivanov, M.; Walters, Z. B.; Smirnova, O. Time-dependent analytical R-matrix approach for strong-field dynamics. II. Many-electron systems. *Phys. Rev. A: At., Mol., Opt. Phys.* **2012**, *86*, 043409.
- (20) Bauch, S.; Sorensen, L. K.; Madsen, L. B. Time-dependent generalized-active-space configuration-interaction approach to photoionization dynamics of atoms and molecules. *Phys. Rev. A: At., Mol., Opt. Phys.* **2014**, *90*, 062508.
- (21) Krause, P.; Schlegel, H. B. Angle-dependent ionization of small molecules by time-dependent configuration interaction and an absorbing potential. *J. Phys. Chem. Lett.* **2015**, *6*, 2140–2146.
- (22) Krause, P.; Schlegel, H. B. Angle-dependent ionization of hydrides AH_n calculated by time-dependent configuration interaction with an absorbing potential. *J. Phys. Chem. A* **2015**, *119*, 10212–20.
- (23) Liao, Q.; Li, W.; Schlegel, H. B. Angle-dependent strong field ionization of triple bonded systems calculated by time-dependent configuration interaction with an absorbing potential. *Can. J. Chem.* **2016**, *94*, 989.
- (24) Krause, P.; Schlegel, H. B. Strong-field ionization rates of linear polyenes simulated with time-dependent configuration interaction with an absorbing potential. *J. Chem. Phys.* **2014**, *141*, 174104.
- (25) Krause, P.; Sonk, J. A.; Schlegel, H. B. Strong field ionization rates simulated with time-dependent configuration interaction and an absorbing potential. *J. Chem. Phys.* **2014**, *140*, 174113.
- (26) Frisch, M. J.; Trucks, G. W.; Schlegel, H. B.; Scuseria, G. E.; Robb, M. A.; Cheeseman, J. R.; Scalmani, G.; Barone, V.; Mennucci, B.; Petersson, G. A.; et al. *Gaussian Development Version*, revision H.20+; Gaussian Inc.: Wallingford, CT, 2010.
- (27) Dunning, T. H. Gaussian-basis sets for use in correlated molecular calculations. I. The atoms boron through neon and hydrogen. *J. Chem. Phys.* **1989**, *90*, 1007–1023.
- (28) Wilson, A. K.; van Mourik, T.; Dunning, T. H. Gaussian basis sets for use in correlated molecular calculations. VI. Sextuple zeta correlation consistent basis sets for boron through neon. *J. Mol. Struct.: THEOCHEM* **1996**, *388*, 339–349.